

The helicity constraint in turbulent dynamos with shear

Axel Brandenburg,^{1,2★} Alberto Bigazzi³ and Kandaswamy Subramanian⁴

¹NORDITA, Blegdamsvej 17, DK-2100 Copenhagen Ø, Denmark

²Department of Mathematics, University of Newcastle upon Tyne, NE1 7RU

³Department of Mathematics, Politecnico di Milano, Piazza Leonardo da Vinci 32, I-20133 Milano, Italy

⁴National Centre for Radio Astrophysics – TIFR, Poona University Campus, Ganeshkhind, Pune 411 007, India

Accepted 2001 February 26. Received 2001 January 8; in original form 2000 November 6

ABSTRACT

The evolution of magnetic fields is studied using simulations of forced helical turbulence with strong imposed shear. After some initial exponential growth, the magnetic field develops a large-scale travelling wave pattern. The resulting field structure possesses magnetic helicity, which is conserved in a periodic box by the ideal magnetohydrodynamics equations and can hence only change on a resistive time-scale. This strongly constrains the growth time of the large-scale magnetic field, but less strongly constrains the length of the cycle period. Comparing this with the case without shear, the time-scale for large-scale field amplification is shortened by a factor Q , which depends on the relative importance of shear and helical turbulence, and which also controls the ratio of toroidal to poloidal field. The results of the simulations can be reproduced qualitatively and quantitatively with a mean-field $\alpha\Omega$ -dynamo model with alpha-effect and turbulent magnetic diffusivity coefficients that are less strongly quenched than in the corresponding α^2 -dynamo.

Key words: magnetic fields – MHD – turbulence.

1 INTRODUCTION

In astrophysical bodies such as stars and galaxies there is a large-scale strong magnetic field. Such fields have usually significant magnetic helicity (e.g. Pevtsov, Canfield & Metcalf 1995; Berger & Ruzmaikin 2000). This is non-trivial, because magnetic helicity is a conserved quantity and can only change if there is a flux of helicity through the boundaries, or through resistive effects which are however very slow. Although this has been known for some time, it has only recently been identified as the fundamental reason for ‘catastrophic’ quenching of the α -effect in mean-field dynamo theory (Blackman & Field 2000; Kleeorin et al. 2000). Simulations of non-mirror symmetric turbulence, which is prototypical of flows producing α^2 -dynamos, has shown that a large-scale helical magnetic field can only grow to its final (super-) equipartition field strength on a *resistive* time-scale (Brandenburg 2001, hereafter B2001).

One may be tempted to ignore the problem of helicity conservation because it has mainly been discussed in connection with rather idealized models. We believe, however, that the problem is serious and quite general. In fact, it also applies to convection-driven dynamos and even to the case where the dynamo-generating flow is the result of magnetic instabilities, as was found to be the case in simulations of accretion discs with a dynamo-generated large-scale field (Brandenburg et al. 1995). This

may be particularly surprising considering the rather plausible expectation that the α -effect and turbulent diffusivity should be ‘anti-quenched’ and should increase with increasing field strength (Hasler, Kaisig & Rüdiger 1995; Brandenburg, Saar & Turpin 1998). If such a mechanism is to be successful, it must still obey helicity conservation and can then only produce a field with vanishing net magnetic helicity.

There is strong observational evidence that the solar magnetic field is indeed helical (Seehafer 1990; Pevtsov et al. 1995). These observations suggest negative current helicity of the small-scale fields in the northern hemisphere. Using a relation obtained by Keigns (1983), this implies a positive α -effect (Seehafer 1996), which is consistent with B2001. In order to produce finite net-helicity one must get rid of fields with opposite signs of magnetic helicity, either through dissipation (which is slow) or through selective losses through open boundaries. So far however there is no evidence from simulations that such losses involve fields of significant strength and opposite sign of magnetic helicity relative to those that remain in the dynamo-active domain (Brandenburg & Dobler 2001).

The dynamo simulations that allowed consideration of the question of the helicity constraint were all of α^2 -type, so there was no additional field amplification by shear. Thus, an outstanding question is whether or not the helicity constraint also plays a role in the presence of shear through which strong toroidal magnetic fields can be generated without affecting the magnetic helicity.

There are a number of working dynamos which have both open

★E-mail: brandenb@nordita.dk

boundaries and shear (e.g. Brandenburg et al. 1995; Glatzmaier & Roberts 1995), but those models are rather complex and use subgrid-scale modelling, so, one cannot straightforwardly define an effective magnetic Reynolds number. This makes a reliable assessment of the effects of helicity conservation difficult. Nevertheless, it clearly remains one of the next important tasks to reconsider these or similar simulations in the light of helicity conservation. In order to determine the relative importance of the various possibilities for relaxing the helicity constraint (shear, open boundaries, etc.) it is useful to consider each possibility in isolation. As a straightforward extension of the model of B2001 we consider here the inclusion of large-scale sinusoidal shear, which allows us to retain the assumption of periodic boundary conditions.

We have mentioned already that shear could be important for relaxing the helicity constraint because the toroidal field generated by stretching does not need to be helical and hence would not be subject to the helicity constraint. On the other hand, shear alone is insufficient for dynamo action: one needs an additional effect that regenerates poloidal (cross-stream) field from toroidal field (e.g. Moffatt 1978; Krause & Rädler 1980). The main point of the present paper is to show that, even though much of the magnetic field amplification is due to shear, which causes the field to be only weakly helical, the magnetic field is still subject to a (modified) helicity constraint. More specifically, we shall show that it is no longer the large-scale field as such which grows resistively, but rather the *geometrical mean* of the magnitudes of the poloidal and toroidal mean fields. The reason is simple: large-scale helicity measures essentially the linkage of poloidal and toroidal fields and must therefore be proportional to the product of the two. The constraint that helicity can change only on a resistive time-scale can then be alleviated. This is because, now, for the same magnetic helicity, stronger toroidal fields are possible at the expense of weaker poloidal fields. Conversely, equipartition strength large-scale fields can be attained in shorter times by the ratio of toroidal to poloidal field strength.

2 THE MODEL

As in B2001 we adopt the magnetohydrodynamics (MHD) equations for an isothermal compressible gas, driven by a given body force \mathbf{f} , which represents both shear and small-scale driving:

$$\frac{D \ln \rho}{Dt} = -\nabla \cdot \mathbf{u}, \quad (1)$$

$$\frac{D\mathbf{u}}{Dt} = -c_s^2 \nabla \ln \rho + \frac{\mathbf{J} \times \mathbf{B}}{\rho} + \frac{\mu}{\rho} \left(\nabla^2 \mathbf{u} + \frac{1}{3} \nabla \nabla \cdot \mathbf{u} \right) + \mathbf{f}, \quad (2)$$

$$\frac{\partial \mathbf{A}}{\partial t} = \mathbf{u} \times \mathbf{B} - \eta \mu_0 \mathbf{J}, \quad (3)$$

where $D/Dt = \partial/\partial t + \mathbf{u} \cdot \nabla$ is the advective derivative, \mathbf{u} is the velocity, ρ is the density, $\mathbf{B} = \nabla \times \mathbf{A}$ is the magnetic field, \mathbf{A} is its vector potential, $\mathbf{J} = \nabla \times \mathbf{B}/\mu_0$ is the current density, η is the magnetic diffusivity, and μ is the dynamical viscosity. We adopt a forcing function \mathbf{f} of the form

$$\mathbf{f} = \mathbf{f}_{\text{turb}} + \mathbf{f}_{\text{shear}}, \quad (4)$$

where

$$\mathbf{f}_{\text{shear}} = C_{\text{shear}} \frac{\mu}{\rho} \hat{\mathbf{y}} \sin x \quad (5)$$

balances the viscous stress once a sinusoidal shear flow has been

established, and

$$\mathbf{f}_{\text{turb}} = \text{Re}\{N\mathbf{f}_{k(t)} \exp[i\mathbf{k}(t) \cdot \mathbf{x} + i\phi(t)]\} \quad (6)$$

is the small-scale helical forcing with

$$\mathbf{f}_k = \frac{\mathbf{k} \times (\mathbf{k} \times \hat{\mathbf{e}}) - i|\mathbf{k}|(\mathbf{k} \times \hat{\mathbf{e}})}{2k^2 \sqrt{1 - (\mathbf{k} \cdot \hat{\mathbf{e}})^2/k^2}}. \quad (7)$$

Here $\hat{\mathbf{e}}$ is an arbitrary unit vector required to generate a vector $\mathbf{k} \times \hat{\mathbf{e}}$ that is perpendicular to \mathbf{k} , $\phi(t)$ is a random phase, and $N = f_0 c_s (k c_s / \delta t)^{1/2}$, where f_0 is a non-dimensional factor, $k = |\mathbf{k}|$, and δt is the length of the time-step. As in B2001 we focus on the case where $|\mathbf{k}|$ is around $k_f \equiv 5$, and select randomly at each time-step one of the 350 possible vectors in the range $4.5 < |\mathbf{k}| < 5.5$.

We use non-dimensional units where $c_s = k_1 = \rho_0 = \mu_0 = 1$. Here, c_s is the speed of sound, k_1 is the smallest wavenumber in the box (so its size is 2π), ρ_0 is the mean density (which is conserved), and μ_0 is the vacuum permeability.

We are interested in the case where shear is strong compared with the turbulence, but still subsonic. In B2001 we used $f_0 = 0.1$ and found that the resulting Mach number of the turbulence was between 0.1 and 0.3, which is already so close to unity that there would be no room to accommodate sufficiently large shear which is still subsonic. Thus, we now choose f_0 to be 10 times smaller, and we take $f_0 = 0.01$. During the saturated phase of the dynamo the resulting rms velocities in the meridional (xz) plane are now around 0.015. For the shear parameter we choose $C_{\text{shear}} = 1$, corresponding to the velocity shear $S_0 = 1$, where $S = \partial u_y / \partial x$ and the subscript 0 indicates the absence of other effects such as turbulence and magnetic forces. In practice the resulting velocity shear is smaller; $S = 0.6$. Since the size of the domain is 2π , the toroidal rms velocities are also around 0.6, which is about 40 times stronger than the velocities in the meridional plane. The rms velocity from wavenumbers $k \geq 2$ is 0.035, and this is also the value that we shall use for our estimates of the magnetic Reynolds number and the equipartition field strength.

We choose a magnetic Prandtl number of 10, i.e. $\mu/(\rho_0 \eta) = 10$, and use $\eta = 5 \times 10^{-4}$, so that the magnetic Reynolds number based on the box size ($= 2\pi$) is about 400. The magnetic Reynolds number based on the forcing scale is about 80. The kinetic Reynolds number based on the forcing scale is only eight, so one cannot expect a proper inertial range. The turnover time based on the forcing scale is $\tau = 40$. In the following we denote by poloidal and toroidal components those in the xz plane and the y direction, respectively.

As usual for these type of simulations with helical forcing, there is strong dynamo action at small scales amplifying an initially weak random seed magnetic field exponentially (on a dynamical time-scale) to equipartition with kinetic energy. The poloidal field, which is strongly dominated by small scales, saturates early on (at $t \approx 1000$) at a level of about 0.010–0.015. The toroidal field saturates later (at $t \approx 2000$) at a level of about 0.2–0.3, and is then already dominated by large scales.

We begin by discussing the resulting field structure at late times, and then turn to the question of resistively limited growth of the large-scale field, and finally make comparisons with the $\alpha\Omega$ -dynamo theory.

3 FIELD STRUCTURE

In Fig. 1 we show images of the three field components in the meridional plane. Note that the toroidal field shows much smoother

and larger-scale structures than the meridional field components. Moreover, the toroidal field shows almost no variation along the y direction: the toroidal average, \bar{B}_y , (second row), is very similar to an individual meridional cross-section of B_y (first row). However, in contrast to the case without shear, where the mean fields showed systematic variations only in one of the three coordinate directions (B2001), here the toroidal field varies with both x and z , consisting of a superposition of modes with $k_x = 1$ and $k_z = 1$.

The toroidal component of the mean field displays dynamo waves travelling in opposite directions at different x positions, depending on the local sign of the shear. For $x = -\pi$ the local shear is negative and the dynamo wave travels in the positive z direction, whilst for $x = 0$ the local shear is positive and the wave travels in the negative z direction (at least after $t = 4000$); see Fig. 2. This is consistent with what is predicted from mean-field $\alpha\Omega$ -dynamo theory (e.g. Yoshimura 1975). The dynamo wave at $x = -\pi$ is quite well established at $t = 2000$, but the behaviour at $x = 0$ is more complicated, and a clear dynamo wave develops only after $t = 4000$. The cycle period at $x = 0$ is also longer than at $x = -\pi$. This complicated behaviour suggests that the turbulence properties may not be homogeneous in x , which could be a consequence of the magnetic feedback.

There is a systematic phase shift and a well-defined amplitude ratio between B_y and B_x ; see Fig. 3. Note also that the dynamo wave

is markedly non-harmonic. These are clear properties that can be compared with the mean-field model calculations (Section 6).

Before we turn to the saturation of the field at the scale of the box we first want to assess the relative importance of the different Fourier modes at different times. Thus, we plot in Fig. 4 the evolution of the power, $|\hat{B}_i(k_j)|^2$, in a few selected modes. Note that after $t = 1700$, most of the power is in the mode $|\hat{B}_y(k_z)|^2$, i.e. the toroidal field component with variation in the z direction. Between $t = 1700$ and ≈ 3500 the ratio of toroidal to poloidal field energies is around 10^4 , so $B_{\text{tor}}/B_{\text{pol}} \approx 50$. At later times this ratio diminishes. This may suggest that there is a growing contribution from α^2 -type dynamo action. This is also supported by the apparently independent evolution of the oscillatory k_z -mode and the non-oscillatory k_x -mode; see Fig. 4.

In Fig. 5 we show the two-dimensional power spectra of the three components of the mean field, $\bar{\mathbf{B}}$. (Here and elsewhere we use denote y -averaged fields by a bar, whilst angular brackets are used for full volume averages.) Note that first a strong toroidal field builds up, and at later times the poloidal field components also gain significant power at the largest scale (i.e. at $k^2 < 2$). One should bear in mind, however, that these spectra are for the *mean* fields. The three-dimensional power spectra of the non-averaged fields reveal that the poloidal fields are ‘noisy’ and possess significant power at the forcing wavenumber, k_f ; see Fig. 6.

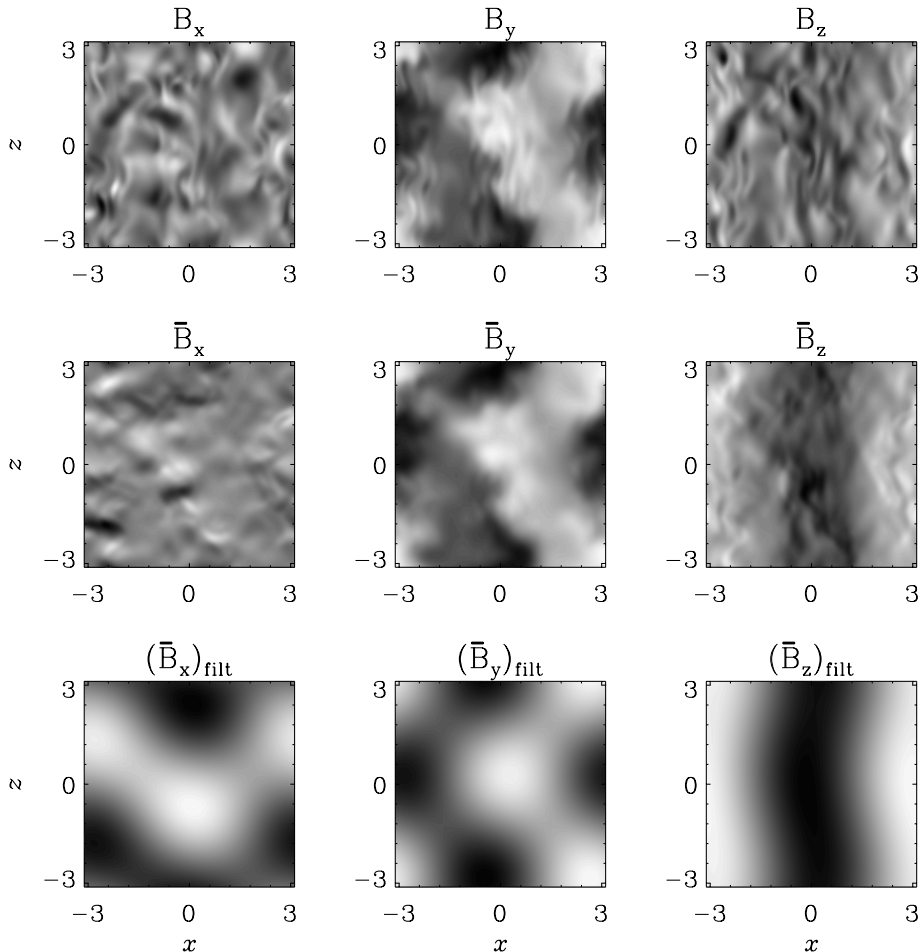


Figure 1. Images of the three components of \mathbf{B} in an arbitrarily chosen xz plane (first row), compared with the y -averaged fields (second row) and the Fourier-filtered y -averaged fields with $|k| \leq 2$, indicated by the subscript ‘filt’ (third row). Dark (light) shadings refer to negative (positive) values. 120^3 meshpoints, $t = 6000$.

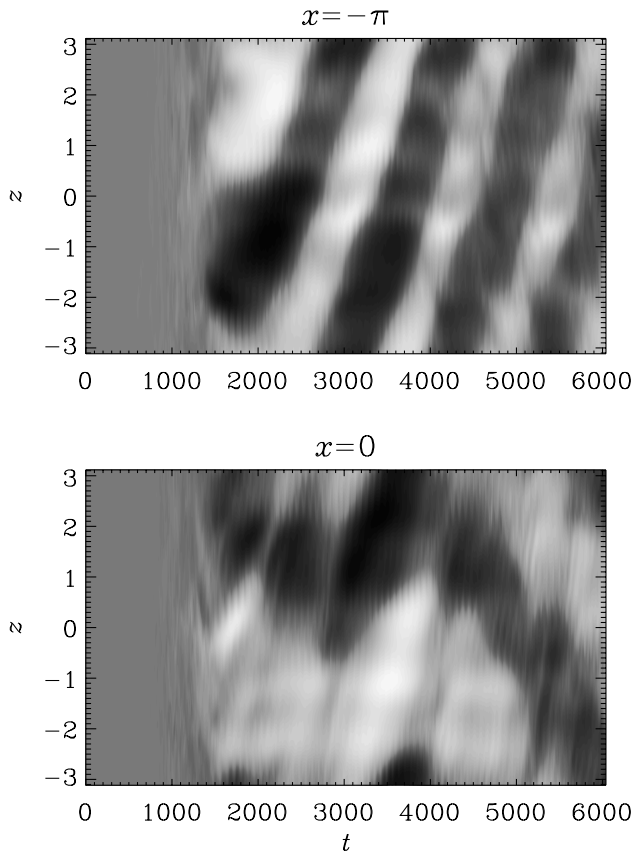


Figure 2. Space–time diagram of the mean toroidal field at $x = -\pi$ (negative local shear) and $x = 0$ (positive local shear). Dark (light) shadings refer to negative (positive) values. Note the presence of dynamo waves travelling in the positive (negative) z direction for negative (positive) local shear.

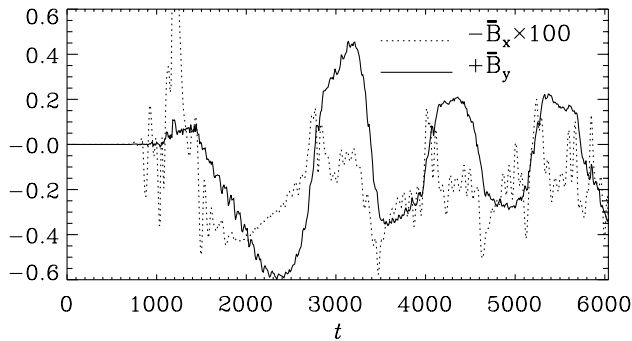


Figure 3. Evolution of \bar{B}_x and \bar{B}_y at $x = -\pi$ and $z = 0$. Note that \bar{B}_x has been scaled by a factor -100 .

The small-scale contributions to the poloidal field result from variations in the toroidal direction, as can be seen in a longitudinal cross-section; see Fig. 7, where we show images of the three field components in the yz plane. The figure shows that whilst the toroidal field is relatively coherent in the toroidal direction, the poloidal field components are much less coherent and show significant fluctuations in the y direction.

We now turn to the temporal evolution of the resulting large-scale magnetic field that gradually emerges during this simulation. We begin by briefly reviewing the main results in the absence of shear (B2001).

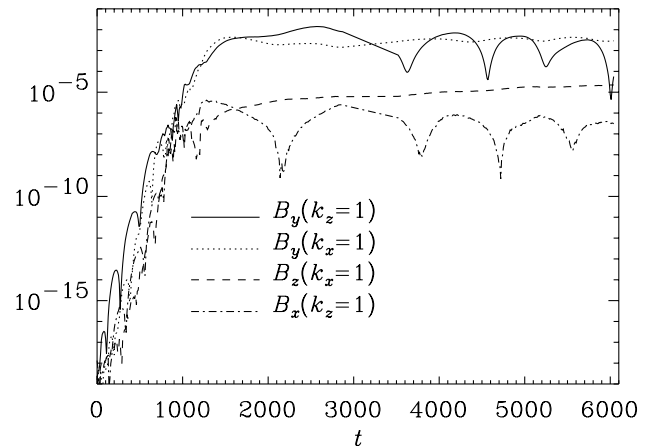


Figure 4. Evolution of the power, $|\hat{B}_i(k_j)|^2$, of a few selected Fourier modes. After $t = 1700$, most of the power is in the mode $|\hat{B}_y(k_z)|^2$, i.e. in the toroidal field component with variation in the z direction.

4 RESISTIVELY LIMITED GROWTH ON LARGE SCALES

In an unbounded or periodic system the magnetic helicity, $\langle \mathbf{A} \cdot \mathbf{B} \rangle$, can only change if there is microscopic magnetic diffusion, η , and finite current helicity, $\langle \mathbf{J} \cdot \mathbf{B} \rangle$,

$$\frac{d}{dt} \langle \mathbf{A} \cdot \mathbf{B} \rangle = -2\eta \langle \mathbf{J} \cdot \mathbf{B} \rangle. \quad (8)$$

In B2001, a possible configuration for the large-scale magnetic field was

$$\bar{\mathbf{B}} = B_0 \begin{pmatrix} \cos(k_1 z + \varphi_x) \\ \sin(k_1 z + \varphi_y) \\ 0 \end{pmatrix}, \quad (9)$$

which corresponds to a force-free magnetic field that varies in the z direction, although variations in one of the other two coordinate directions, and with arbitrary phase shifts φ_x ($\approx \varphi_y$), were also possible (B2001). $B_0 = \langle \bar{\mathbf{B}}^2 \rangle^{1/2}$ is the amplitude, whose time dependence was found to be subject to the helicity constraint (B2001).

The present case is different because of the shear which tends to increase the toroidal field, but not the poloidal field. We model this by writing

$$\bar{\mathbf{B}} = \begin{pmatrix} B_{\text{pol}} \cos(k_1 z + \varphi_x) \\ B_{\text{tor}} \sin(k_1 z + \varphi_y) \\ 0 \end{pmatrix}, \quad (10)$$

where B_{pol} and B_{tor} are the amplitudes of the poloidal and toroidal field components. In addition to the z dependence there can also be an x dependence of the mean field, which is natural due to the x dependence of the imposed shear profile. However, for the following argument all we need is the fact that the magnetic and current helicities are proportional to the product of poloidal and toroidal field magnitudes,

$$\langle \mathbf{J} \cdot \bar{\mathbf{B}} \rangle / k_1 \approx \mp B_{\text{tor}} B_{\text{pol}} \approx k_1 \langle \bar{\mathbf{A}} \cdot \bar{\mathbf{B}} \rangle. \quad (11)$$

The upper sign applies to the present case where the kinetic helicity is positive (representative of the southern hemisphere), and the

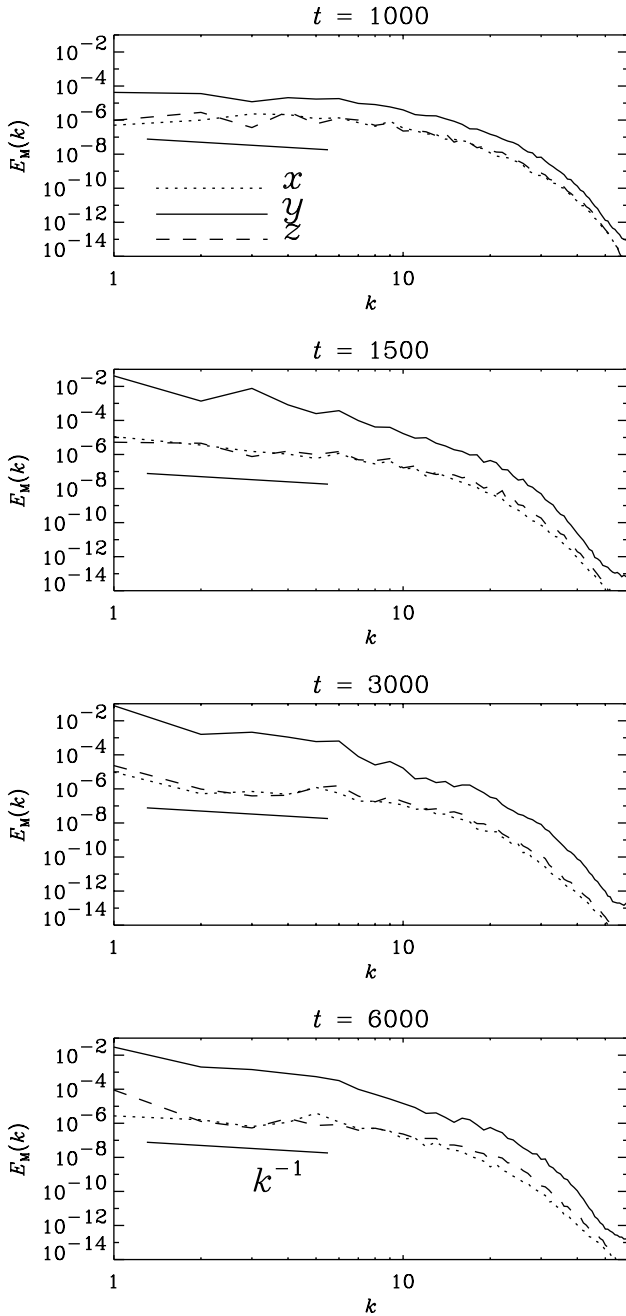


Figure 5. Two-dimensional power spectra of the three components of the mean field, $\bar{\mathbf{B}}_y$ (solid for the y component, and broken lines for the x and z components). The k^{-1} slope is given for comparison.

approximation becomes exact if the field is indeed represented by equation (10).

Following B2001, in the steady case $\langle \mathbf{A} \cdot \mathbf{B} \rangle = \text{constant}$, see equation (8), and so the right-hand side of equation (8) must vanish, i.e. $\langle \mathbf{J} \cdot \mathbf{B} \rangle = 0$, which can only be consistent with equation (11) if there is a small-scale component, $\langle \mathbf{j} \cdot \mathbf{b} \rangle$, whose sign is opposite to that of $\langle \mathbf{J} \cdot \bar{\mathbf{B}} \rangle$. Hence we write

$$\langle \mathbf{J} \cdot \mathbf{B} \rangle = \langle \mathbf{J} \cdot \bar{\mathbf{B}} \rangle + \langle \mathbf{j} \cdot \mathbf{b} \rangle \approx 0. \quad (12)$$

This yields, analogously to B2001,

$$-\frac{d}{dt}(B_{\text{tor}}B_{\text{pol}}) = +2\eta k_1^2(B_{\text{tor}}B_{\text{pol}}) - 2\eta k_1 \langle \mathbf{j} \cdot \mathbf{b} \rangle, \quad (13)$$

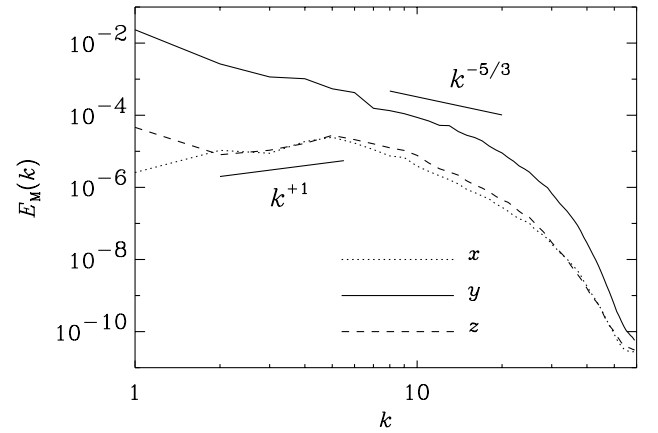


Figure 6. Three-dimensional power spectrum of the three field components. 120^3 meshpoints, $t = 6000$.

which yields the solution

$$B_{\text{tor}}B_{\text{pol}} = \epsilon_0 B_{\text{eq}}^2 [1 - e^{-2\eta k_1^2(t-t_s)}], \quad (14)$$

where $\epsilon_0 = \langle \mathbf{j} \cdot \mathbf{b} \rangle / (k_1 B_{\text{eq}}^2)$ is a pre-factor, B_{eq} is the equipartition field strength with $B_{\text{eq}}^2 = \mu_0 \langle \rho u^2 \rangle$, and t_s is the time when the small-scale field has saturated, which is when equation (13) becomes applicable. All this is equivalent to B2001, except that $\langle \bar{\mathbf{B}}^2 \rangle$ is now replaced by the product of B_{tor} and B_{pol} . The significance of this expression is that large toroidal fields are now possible if the poloidal field is weak.

In order to compare with the simulation we now define

$$B_{\text{tor}} \equiv \langle \bar{\mathbf{B}}_y^2 \rangle^{1/2}, \quad B_{\text{pol}} \equiv \langle \bar{\mathbf{B}}_x^2 + \bar{\mathbf{B}}_z^2 \rangle^{1/2}. \quad (15)$$

Note that this definition generalizes that given in equation (10). In Fig. 8 we show the evolution of B_{tor} and B_{pol} , and compare the evolution of the product $B_{\text{tor}}B_{\text{pol}}$ with equation (14). There are different stages: for $1200 < t < 2200$ and $3000 < t < 3700$ the effective value of k_1^2 is $k_1^2 = 2$ (because there are contributions from $k_x = 1$ and $k_z = 1$; see Fig. 4), whilst at other times ($2500 < t < 2800$ and $t > 4000$) the contribution from $k_x = 1$ (for $2500 < t < 2800$) or $k_z = 1$ (for $t > 4000$) has become subdominant and we have effectively $k_1^2 = 1$. This is consistent with the change of field structure discussed in Section 3: for $2000 < t < 3000$ and around $t = 4000$ the $B_y(k_x = 1)$ mode is less powerful than the $B_y(k_z = 1)$ mode.

We may conclude that the effect of the helicity constraint is clearly identified in the present simulation. This is substantiated by the fit shown in Fig. 8. The episodes during which the field amplitude is below that obtained from the helicity constraint can be explained by temporary changes in the field geometry.

5 ASTROPHYSICAL IMPLICATIONS

The main result of this paper is a quantitative modification of the helicity constraint for dynamos in the presence of shear. With shear included the estimate for $\langle \bar{\mathbf{B}}^2 \rangle$ of B2001 is now to be replaced by the product $B_{\text{tor}}B_{\text{pol}} \approx \langle \bar{\mathbf{B}}^2 \rangle / Q$, where $Q = B_{\text{tor}}/B_{\text{pol}} \gg 1$ and so $\langle \bar{\mathbf{B}}^2 \rangle \approx B_{\text{tor}}^2$. For *early times*, the exponential function in equation (14) can be expanded:

$$\langle \bar{\mathbf{B}}^2 \rangle \approx \epsilon_0 B_{\text{eq}}^2 2\eta k_1^2 (t - t_s) Q. \quad (16)$$

In the case of efficient large-scale dynamo action the small-scale current helicity is very nearly equal to the normalized kinetic

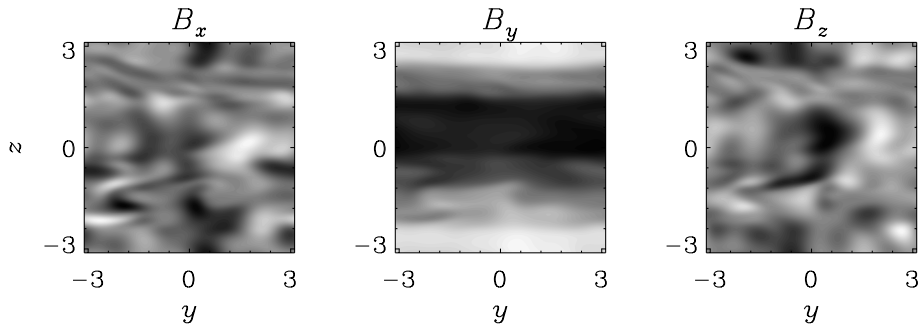


Figure 7. Images of the three components of \mathbf{B} in an arbitrarily chosen yz plane. Dark (light) shadings refer to negative (positive) values. Note that B_x and B_z show strong variations in y , but B_y does not. $t = 6000$.

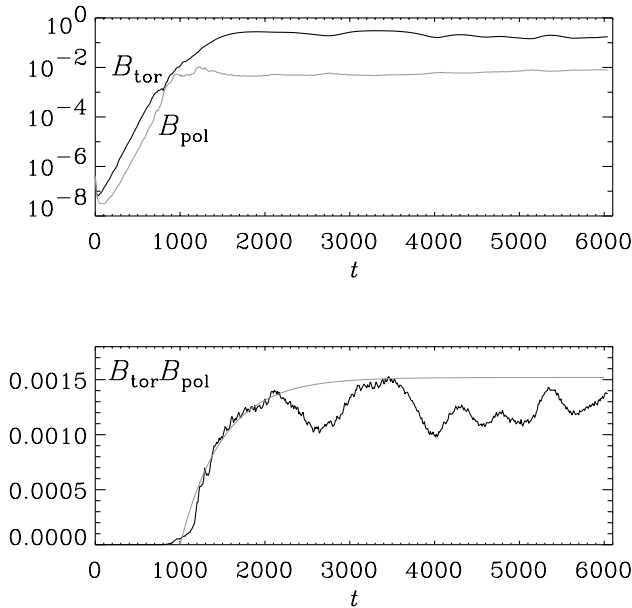


Figure 8. Growth of poloidal and toroidal magnetic fields on a logarithmic scale (upper panel), and product of poloidal and toroidal magnetic fields on a linear scale. For the fit we have used $k_1^2 = 2$, $B_{\text{eq}} = 0.035$, and $\epsilon_0 = 1.3$.

helicity, $\rho_0 \langle \boldsymbol{\omega} \cdot \mathbf{u} \rangle$ (see also Brandenburg & Subramanian 2000), which in turn is approximately $k_f \langle \rho \mathbf{u}^2 \rangle$. Since $\epsilon_0 = \langle \mathbf{j} \cdot \mathbf{b} \rangle / (k_1 B_{\text{eq}}^2)$, this leads to $\epsilon_0 \approx k_f / k_1$, which is 5 in the present case. The value of ϵ_0 that fits the simulation results best is only 1.3 (see Fig. 8), so the dynamo does not seem to be fully efficient. This reduced efficiency could partly be explained by the fact that the actual field is not sinusoidal, as assumed in equation (10), and that the phase shift between poloidal and toroidal fields is not optimal.

We now want to estimate the time, τ_{eq} , required to build up a large-scale field of equipartition field strength, i.e. $\langle \bar{\mathbf{B}}^2 \rangle = B_{\text{eq}}^2$. In units of the turnover time, $\tau = L/u_{\text{rms}}$, we have

$$\tau_{\text{eq}}/\tau = u_{\text{rms}} L / (2\eta k_1^2 L^2 \epsilon_0 Q) = R_m / (\epsilon_1 Q), \quad (17)$$

where we have introduced a new coefficient $\epsilon_1 = 2\epsilon_0 k_1^2 L^2$. Applying this to the Sun we have $\tau_{\text{eq}}/\tau \approx 10^4 - 10^7$, if we assume $R_m = 10^8 - 10^{10}$, $Q = 10 - 100$, and $\epsilon_1 \approx 2(2\pi)^2 \approx 100$. At the bottom of the solar convection zone the turnover time is about 10 d (0.03 yr), so the time-scale for building up a large-scale field for equipartition strength is between 300 and 3×10^5 yr.

We have not yet studied models with different values of the magnetic Reynolds number, so we cannot properly assess the effect

on the cycle period. If the cycle period scales in the same way as the growth time of the dynamo, then the helicity constraint would, even in the presence of shear, continue to pose a serious problem for understanding cyclic activity of solar-like stars. However, before making more detailed comparisons with astrophysical bodies it would be necessary, for example, to assess the importance of open boundaries. This now seems to be one of the most important aspects remaining to be clarified in the theory of large-scale dynamos [see also Blackman & Field (2000) and Kleeorin et al. (2000)]. Although initial results from simulations with open boundaries seem pessimistic in that respect (Brandenburg & Dobler 2001), the effects of open boundaries are likely to be more important in cases with outflows (e.g. in protostellar accretion discs or in active galactic nuclei). It should also be mentioned that large-scale dynamos may operate with non-helical flows; see the recent papers by Vishniac & Cho (2001) and Zheligovsky, Podvigina & Frisch (2000). This may relax the helicity constraint, but so far there are no simulations supporting this possibility.

6 MEAN-FIELD INTERPRETATION

In the absence of shear, the results of the simulations could be well modelled in terms of a mean-field α^2 -dynamo with simultaneous quenching of the α -effect and the turbulent diffusivity. In this section we shall try to do the same for the $\alpha\Omega$ -dynamo. Since the shear is strong compared with the inverse turnover-time we can make the $\alpha\Omega$ -approximation, i.e. we can neglect the α -effect in the equation for the generation of the toroidal magnetic field. We also assume that the magnetic field varies only in the direction of the vorticity vector of the shear, which is the direction in which the dynamo wave travels (Yoshimura 1975). In the present case this is the z direction. Thus, the relevant equations in terms of the mean vector potential $\bar{\mathbf{A}}$, are

$$\partial_t \bar{A}_x = -S \bar{A}_y + \eta_T \partial_z^2 \bar{A}_x, \quad (18)$$

$$\partial_t \bar{A}_y = +\alpha \bar{B}_y + \eta_T \partial_z^2 \bar{A}_y, \quad (19)$$

where $\bar{B}_y = \partial_z \bar{A}_x$ and $\eta_T = \eta + \eta_t$ is the *total* (microscopic plus turbulent) magnetic diffusivity. [In equation (18) we have used a particular gauge that allowed us to write the shear term as $S \bar{A}_y$; see Brandenburg et al. (1995) for details.] As in the case of the α^2 -dynamo, we shall assume that η_t and α are quenched in the same way:

$$\alpha = \frac{\alpha_0}{1 + \alpha_B \bar{\mathbf{B}}^2 / B_{\text{eq}}^2}, \quad \eta_t = \frac{\eta_0}{1 + \eta_B \bar{\mathbf{B}}^2 / B_{\text{eq}}^2}, \quad (20)$$

where $\alpha_B = \eta_B$ is assumed, and $\bar{\mathbf{B}}^2 = \bar{B}_x^2 + \bar{B}_y^2$ with $\bar{B}_x = -\partial_z \bar{A}_y$.

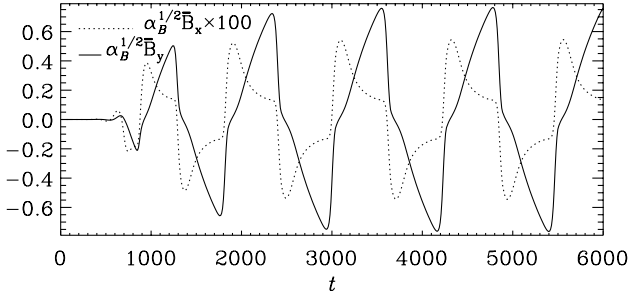


Figure 9. Evolution of $\alpha_B^{1/2} \bar{B}_x$ and $\alpha_B^{1/2} \bar{B}_y$ in the one-dimensional mean-field model with $\mathcal{D} = 10$, $\lambda = 0.015$ and $\eta = 5 \times 10^{-4}$. Note that \bar{B}_x has been scaled by a factor 100. (In this case $S > 0$, so we have plotted $+\bar{B}_x$, and not $-\bar{B}_x$ as we did in Fig. 3 where $S < 0$.)

In the case of the α^2 -dynamo in a periodic domain the two components of the magnetic field were sinusoidal and phase shifted by 90° such that $\bar{\mathbf{B}}^2$ was spatially constant. It was therefore possible to obtain the solution for the evolution of $\bar{\mathbf{B}}^2$ in closed form. The final saturation field strength, B_{fin} , was then given by [equation (55) of B2001]

$$\alpha_B \frac{B_{\text{fin}}^2}{B_{\text{eq}}^2} \approx \frac{\lambda}{\eta k_1^2} \quad (\text{for the } \alpha^2\text{-dynamo}), \quad (21)$$

where $\lambda = \alpha_0 k_1 - \eta_{T0} k_1^2$ is the kinematic growth rate of the α^2 -dynamo.

In the present case of an $\alpha\Omega$ -dynamo, $\bar{\mathbf{B}}^2$ is no longer spatially constant and the solution cannot be obtained in closed form. We therefore resort to numerical solutions of equations (18)–(20) using periodic boundary conditions. All the solutions turned out to be oscillatory with a period T , but the temporal structure is strongly non-harmonic; see Fig. 9. Note that the time dependence of \bar{B}_x and \bar{B}_y is qualitatively and quantitatively similar to that found in the actual simulation (Fig. 3). The field amplitude depends on the value of α_B and agrees with that found in the simulation (Fig. 3) if $\alpha_B \approx 2$. The solution also depends on the value of the dynamo number

$$\mathcal{D} = \alpha_0 k_1 S / (\eta_{T0} k_1^2)^2, \quad (22)$$

where $\eta_{T0} = \eta + \eta_0$ is the kinematic value of the total turbulent magnetic diffusivity. For the model shown in Fig. 9 we used $\mathcal{D} = 10$, but if \mathcal{D} is doubled the cycle period also approximately doubles. Thus, $\mathcal{D} = 20$ would be more representative for the dynamo wave at $x = 0$ (cf. Fig. 2).

Although the present analysis is straightforward and indeed quite similar to other $\alpha\Omega$ -dynamos considered in the literature (e.g. Moffatt 1978; Krause & Rädler 1980), a main conceptual difference is that here we consider α and η_t to be quenched in the same way, and that we retain the microscopic magnetic diffusion η which is not quenched.

We have determined the value of $\alpha_B B_{\text{fin}}^2 / B_{\text{eq}}^2$ and the cycle frequency $\omega = 2\pi/T$ as a function of $\lambda / \eta k_1^2$ for different values of the dynamo number \mathcal{D} . The results are shown in Fig. 10. We have checked that the different curves in Fig. 10 depend only on the parameter \mathcal{D} , regardless of the values of α_0 , S and η_{T0} , provided the kinematic growth rate of the linearized form of equations (18) and (19),

$$\lambda = -\eta_{T0} k_1^2 + \sqrt{\alpha_0 k_1 S / 2}, \quad (23)$$

is kept unchanged. Note that it is now this λ that enters the expression $\lambda / \eta k_1^2$, which we have considered as the control parameter for the numerical solutions displayed in Fig. 10.

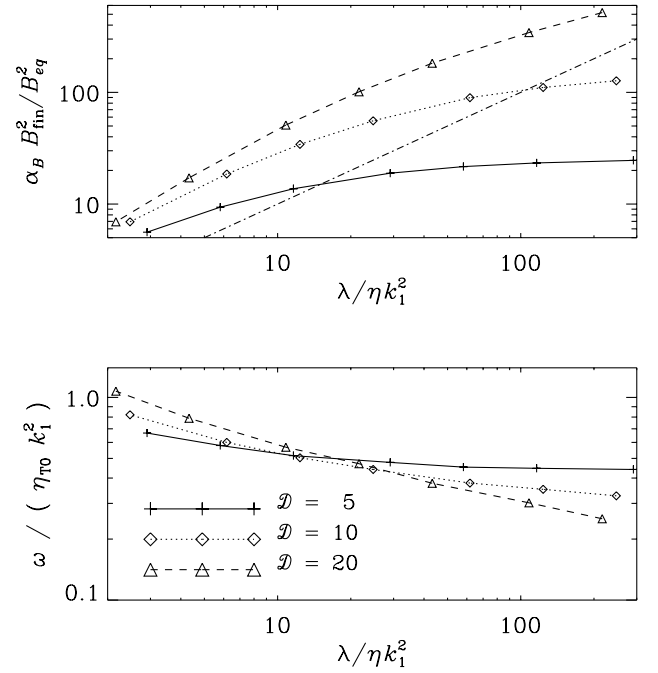


Figure 10. Normalized saturation field strength and cycle frequency for the saturated state of a non-linear one-dimensional $\alpha\Omega$ -dynamo with simultaneous α and η_t quenches. The diagonal (dash-dotted line) in the first panel gives the result for the corresponding α^2 -dynamo (for all values of $\alpha_0 / \eta_{T0} k_1$).

With these preparations we can now make a detailed comparison with the simulation data. In the simulation the kinematic growth rate can be read off the first panel of Fig. 8 and turns out to be $\lambda = 0.015$. Thus, with $\eta = 5 \times 10^{-4}$ and $k_1 = 1$ we have $\lambda / \eta k_1^2 = 30$. From Fig. 10 we see, then, that $\omega / \eta_{T0} k_1^2 \approx 0.4$. For T in the range 1000–2000 we have $\omega = 0.006$ – 0.003 , which yields $\eta_{T0} \approx 0.015$ – 0.0075 , respectively.

Given the values of λ and $\eta_{T0} k_1^2$, we can express the dynamo number as

$$\mathcal{D} / \mathcal{D}_{\text{crit}} = [\lambda / (\eta_{T0} k_1^2) + 1]^2, \quad (24)$$

where $\mathcal{D}_{\text{crit}} = 2$ is the critical value for dynamo action, and we find $\mathcal{D} = 8$ – 18 for $T = 1000$ – 2000 , respectively. From Fig. 10 we see, then, that $\alpha_B B_{\text{fin}}^2 / B_{\text{eq}}^2 = 60$ – 100 . In the simulations we have $B_{\text{fin}} \approx 0.25$ and $B_{\text{eq}} = 0.035$, so $B_{\text{fin}}^2 / B_{\text{eq}}^2 \approx 50$, and therefore $\alpha_B = 1$ – 2 , which is in agreement with the value inferred earlier from the field amplitude; cf. Figs 3 and 9. We can therefore conclude that in an $\alpha\Omega$ -dynamo, α and η_t are quenched much less than in an α^2 -dynamo, where α_B would be around 30. If the weaker quenching for oscillatory $\alpha\Omega$ -type dynamos is confirmed for larger values of the magnetic Reynolds number then this would also suggest that the cycle period is also only weakly increased. Already now the cycle period is closer to the dynamical time-scale than to the resistive one. This is best seen by comparing the two ratios

$$\omega / \eta_{T0} k_1^2 \approx 0.4 \quad \text{and} \quad \omega / \eta k_1^2 \approx 6$$
– $12. \quad (25)$

Note also that the values of $\eta_{T0} k_1^2$ and λ are very close to each other. This confirms again that the turbulent diffusivity is dynamically significant and not quenched to its microscopic value.

Finally we show in Fig. 11 the evolution of $\langle \bar{\mathbf{B}}^2 \rangle / \langle \bar{\mathbf{B}}^2 \rangle_{\text{max}}$ for different values of \mathcal{D} , and compare it with the shape of the curve predicted by the helicity constraint of equation (14). We see that the

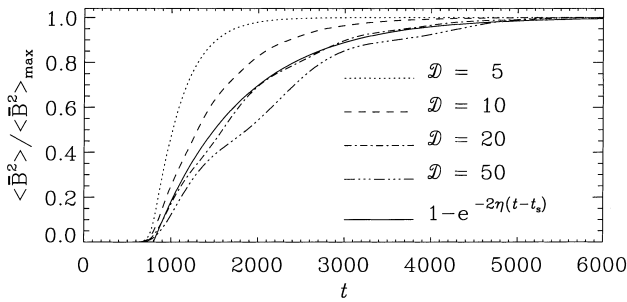


Figure 11. Resistively dominated saturation behaviour in the $\alpha\Omega$ -dynamo for large enough dynamo numbers ($\mathcal{D} \approx 20$). For all curves we have $\lambda = 0.015$ and $\eta = 5 \times 10^{-4}$. For large values of \mathcal{D} the cycle oscillation begins to distort the curve and causes additional deviations from the helicity constraint (solid line), which is best matched for $\mathcal{D} = 20$.

correct shape of the helicity constraint is matched for $\mathcal{D} \approx 20$, which corresponds to the value obtained for $T = 2000$. The fact that the helicity constrained is matched for one particular value of \mathcal{D} is surprising. This suggests that in non-linear $\alpha\Omega$ -dynamo theory the dynamo number is no longer a free parameter, and that there is only one possible value of \mathcal{D} for which the helicity constraint with the correct value of the *microscopic* magnetic diffusivity can be matched.

7 CONCLUSIONS

The present investigations have shown that the effects of the helicity constraint can clearly be identified, even though much of the field amplification results now from the shearing of a poloidal field. Instead of having a constraint on the magnetic energy in the mean field, one now has a constraint on the geometrical mean of the energies in the poloidal and toroidal mean-field components. The dynamo remains time dependent with a typical period that is closer to a dynamical time-scale than to a resistive one. The toroidally averaged field alternates in sign and shows a clear migration pattern.

The present work has revealed that, even though the kinetic helicity of the flow is near its maximum possible value, the poloidal field shows a great deal of ‘noise’, whilst the toroidal field does not. The power spectra of the poloidal field shows that most of the power is in small scales, making the use of averages at first glance questionable. However, once the field is averaged over the toroidal direction the resulting poloidal field is governed by large-scale patterns (the slope of the spectrum is steeper than k^{-1} , which is the critical slope for equipartition of energy between small- and large-scale fields). The presence even of a weak mean poloidal field is crucial for understanding the resulting large-scale field generation in the framework of an $\alpha\Omega$ -dynamo.

The results of the simulations can be reproduced by a mean-field $\alpha\Omega$ -dynamo where the α -effect and turbulent magnetic diffusivity are quenched by the magnetic field. The strength of the quenching is however much weaker than for the corresponding α^2 -dynamo. The resistively limited growth imposed by the magnetic helicity constraint is recovered for one particular value of the dynamo number. Whether or not the cycle period becomes catastrophically large in the limit of large magnetic Reynolds numbers is not entirely clear, because the frequency dependence shown in Fig. 10 seems to level off at a definite value. However, the value of the magnetic Reynolds number where the cycle frequency levels off shifts to larger values as the dynamo number is increased. If it is

confirmed that large magnetic Reynolds numbers (based on the microscopic magnetic diffusivity) also imply large dynamo numbers (based on the value of the turbulent magnetic diffusivity), then the cycle period would probably be too long to explain the cycle periods observed in many late-type stars. On the other hand, using a mean-field model that obeys the magnetic helicity constraint, we found evidence that the cycle period is controlled primarily by the dynamical time-scale.

It is important to remember that the flows considered in the present investigations are driven by some imposed body force. In astrophysical bodies the flows are driven by convection and shear. This does not directly affect the helicity constraint which controls the long time-scales discussed here. However, when open boundary conditions are considered it may be possible that real astrophysical flows have a better ability to dispose of small-scale fields whose magnetic helicity has the opposite sign of that of the large-scale field. [In externally driven flows, open boundaries do not seem to relax the constraint imposed by helicity conservation sufficiently; see Brandenburg & Dobler (2001).]

The driven flows considered here and in related papers have the tremendous advantage of allowing significant progress to be made in understanding the simulation results quantitatively in terms of the mean-field theory. This will be a much harder task for real astrophysical flows. For example, the helicity constraint has, to our knowledge, never been identified in simulations of astrophysically driven flows. This seems to be now one of the most important tasks for future simulations of large-scale dynamos.

ACKNOWLEDGMENTS

We thank Eric Blackman and Anvar Shukurov for many stimulating discussions and comments on the manuscript. We also thank an anonymous referee for making useful suggestions that have led to an improved presentation of the results. ABi and KS acknowledge NORDITA for hospitality during the course of this work. Use of the PPARC supported supercomputers in St Andrews and Leicester is acknowledged.

REFERENCES

- Berger M. A., Ruzmaikin A., 2000, *J. Geophys. Res.*, 105, 10481
- Blackman E. G., Field G. F., 2000, *ApJ*, 534, 984
- Brandenburg A., 2001, *ApJ*, 550, 824 (B2001)
- Brandenburg A., Dobler W., 2001, *A&A*, 369, 329
- Brandenburg A., Subramanian K., 2000, *A&A*, 361, L33
- Brandenburg A., Nordlund Å., Stein R. F., Torkelsson U., 1995, *ApJ*, 446, 741
- Brandenburg A., Saar S. H., Turpin C. R., 1998, *ApJ*, 498, L51
- Glatzmaier G. A., Roberts P. H., 1995, *Nat*, 377, 203
- Hasler K.-H., Kaisig M., Rüdiger G., 1995, *A&A*, 295, 245
- Keinigs R. K., 1983, *Phys. Fluids*, 26, 2558
- Kleeorin N. I., Moss D., Rogachevskii I., Sokoloff D., 2000, *A&A*, 361, L5
- Krause F., Rädler K.-H., 1980, *Mean-Field Magnetohydrodynamics and Dynamo Theory*. Pergamon Press, Oxford
- Moffatt H. K., 1978, *Magnetic Field Generation in Electrically Conducting Fluids*. Cambridge Univ. Press, Cambridge
- Pevtsov A. A., Canfield R. C., Metcalf T. R., 1995, *ApJ*, 440, L109
- Seehafer N., 1990, *Sol. Phys.*, 125, 219
- Seehafer N., 1996, *Phys. Rev. E*, 53, 1283
- Vishniac E. T., Cho J., 2001, *ApJ*, 550, 752
- Yoshimura H., 1975, *ApJ*, 201, 740
- Zheligovsky V. A., Podvigina O. M., Frisch U., Geophys. Astrophys. Fluid Dyn., 2000, nlin.CD/0012005